CrystEngComm

ROYAL SOCIETY OF CHEMISTRY

PAPER

View Article Online
View Journal | View Issue

Cite this: *CrystEngComm*, 2025, **27**, 6295

Exploring bimodal mesoporous aluminum MOFs: synthesis and defect analysis of *rad* net topology with imine-based ligand

Souvik Pal,[a] Ling-I Hung,[a] Wun-Jing Chen,[b] Jiun-Jen Chen,[c] Chun-Chuen Yang[d] and Chia-Her Lin *[ac]

Metal–organic frameworks (MOFs) are a versatile class of porous crystalline materials whose properties can be finely tuned through reticular chemistry. Isoreticular expansion, a powerful strategy for increasing pore size without altering framework topology, has enabled the design of MOFs with hierarchical porosity and enhanced functionality. In this study, we report the scalable synthesis and structural characterization of a new aluminum-based MOF, designated AlDMDA-68, constructed using an imine-based dicarboxylate linker 4,4′-(hydrazine-1,2-iylidenebis(methanylylidene))dibenzoic (H_2DMDA). The framework exhibits a **rad** net analogous to MIL-68(Al), featuring dual-channel architectures with pore diameters up to 3.16 nm. Optimization of reaction parameters, including metal-to-ligand (M/L) ratio, yielded phase-pure materials with rod-like morphology. Powder X-ray diffraction and ^{27}Al MAS NMR confirmed framework formation and the presence of coordination defects, respectively. Nitrogen sorption measurements revealed a high Brunauer–Emmett–Teller (BET) surface area of 1866 m^2 g^{-1} and substantial uptake, indicating a hierarchical microporous–mesoporous structure. The material also demonstrated high thermal stability (~350 °C) and excellent scalability, achieving a fivefold increase in yield without compromising structural integrity. These findings highlight AlDMDA-68 as a promising candidate for various applications and establish elongated imine-based linkers as effective building blocks for designing mesoporous Al-MOFs with tunable functionality.

Received 23rd May 2025,
Accepted 19th August 2025

DOI: 10.1039/d5ce00532a

rsc.li/crystengcomm

Introduction

Metal–organic frameworks (MOFs) constitute a significant class of highly crystalline porous materials that have attracted considerable interest within the scientific community, owing to their remarkable porosity, versatility, and structural integrity.[1–3] One of the primary goals in the field of MOFs is to design and synthesize extensive frameworks with customized structures and properties, which can be effectively achieved through the principles of reticular chemistry.[4] This methodology involves the assembly of secondary building units (SBUs), such as metal clusters, in conjunction with rigid organic linkers that vary in length and geometric configuration. By carefully considering the geometric shapes and chemical compositions of both the SBUs and the organic linkers, researchers can often anticipate the resultant framework topology, particularly when a foundational structure has been established.[5,6] This approach has facilitated the synthesis of various MOFs exhibiting related topologies while differing in terms of pore sizes and volumes, leading to the formation of isoreticular series.[7,8]

The groundbreaking research on isoreticular metal–organic frameworks (IRMOFs) was initiated by Yaghi and his collaborators, who successfully synthesized these innovative materials utilizing octahedral Zn–O SBUs in conjunction with ditopic linkers that preserve a consistent linear geometry while varying in length.[9] Notable examples include 1,4-benzenedicarboxylate (H_2bdc, referred to as IRMOF-1) and biphenyl-4,4′-dicarboxylic acid (H_2bpdc, designated as IRMOF-10), among others. Following this seminal publication, additional isoreticular series of MOFs have arisen, further broadening the scope of the field.[10,11] For instance, Lillerud and colleagues introduced an isoreticular series of zirconium-based MOFs named UiO-66, -67, and -68.[12,13] The UiO series is characterized by a zirconium(IV)-carboxylate cluster, represented as $Zr_6(\mu_3\text{-}O_4)(\mu_3\text{-}OH)_4(CO_2)_{12}$, serving as the SBU. Each SBU is intricately interconnected by twelve dicarboxylate linkers, with UiO-66, -67, and -68 utilizing H_2bdc, H_2bpdc, and 4,4′,4″-

[a] *Department of Chemistry, National Tsing Hua University, Hsinchu, Taiwan. E-mail: chiaher@mx.nthu.edu.tw*
[b] *Department of Chemistry, Chung Yuan Christian University, Taiwan*
[c] *Green Energy and Environment Research Laboratories, Industrial Technology Research Institute, Taiwan*
[d] *Department of Physics, National Central University, Taoyuan City, 32023, Taiwan*

triphenyldicarboxylate (H_2tpdc), respectively, as their linking components. The pioneering aluminum-based MOF (Al-MOF), known as MIL-53, was first documented in 2003 by Férey *et al.*[14] Their innovative work catalyzed a dedicated investigation into Al-MOFs, focusing on the synthesis, characterization, and performance evaluation of various members of the MIL series, which swiftly became a focal point of interest among researchers in the field.[15] Building upon prior research findings, the present study focuses on Al-MOFs, with a specific emphasis on the synthesis of MIL-68(Al), which carries the rad net.[16] The MIL-68 topology was originally prepared by Barthelet *et al.* as a vanadium analogue, recognized for its notably rigid framework, expressed in the formulation $V^{III}(OH)(O_2C–C_6H_4–CO_2)$ for the activated variant of the material.[17] Subsequently, five additional analogues incorporating various metals, including gallium (Ga), indium (In), iron (Fe), aluminum (Al), and scandium (Sc), have been documented.[18–21] These isostructural materials are constructed from infinitely extending linear chains composed of corner-sharing metal-centered octahedra ($MO_4(OH)_2$), where M can represent V, Ga, In, Al, Sc, or Fe. These chains are interconnected through hydroxyl groups and terephthalate ligands, culminating in robust three-dimensional networks. The intriguing structures of these frameworks present two distinct types of channels: one exhibits a pore diameter ranging from 6.0 to 6.4 Å, forming triangular openings, while the other features an opening size between 16 and 17 Å, resulting in hexagonal pores (as illustrated in Fig. S1).[3,16] This unique structural topology, accommodating two varying pore sizes, holds significant potential for the enhancement of gas separation processes. In our research, we have introduced a mesoporous MOF referred to as CYCU-3, synthesized utilizing larger linkers, exemplified by H_2SDC.[3] Notably, MIL-68(Al) and CYCU-3 share the same underlying **rad** net, with CYCU-3 representing an extended analogue featuring two distinct channels of varying configurations. From a topological perspective, CYCU-3 can be regarded as an extended analogue of MIL-68, possessing two distinct channels of varying configurations. Following the removal of extraneous molecules, the cross-sectional dimensions of the hexagonal channel in CYCU-3 measure approximately 28.3 × 31.1 $Å^2$, underscoring its potential in diverse applications driven by structural versatility. The CYCU-3 framework exhibits a substantial pore volume and features open channels with a diameter of 3.0 nm.

When the linker is substituted with a longer H_2TzDB, a new MOF designated as AlTz-68 is obtained, showcasing an impressive hexagonal one-dimensional channel with a remarkable diameter of 3.6 nm.[22] Recently, we introduced another elongated ligand, identified as H_2PDA, to synthesize a new MOF referred to as AlPDA-68.[23] The AlPDA-68 framework features a topology similar to our previous configurations, with notable pore dimensions measuring approximately 4.1 nm. The elongation of bridging ligands has proven to be an effective strategy in the synthesis of new MOFs characterized by mesoporosity. In this context, cost-effective imine ligand, H_2DMDA, with lengths of 15.4 Å, respectively, presents significant advantages over conventional linear organic O-donor ligands, such as the commonly utilized 1,4-benzenedicarboxylic acid (7.7 Å in length). These elongated ligands hold considerable promise for the development of zirconium-based MOFs, providing opportunities for enhanced structural characteristics.[24]

Over the past decade, defect engineering has emerged as a powerful and transformative methodology within the domain of MOF chemistry.[25] This transition signifies a considerable evolution in our understanding of MOFs, shifting from the traditional perspective that views these materials as ideal, rigid structures to an acknowledgment of their dynamic nature, wherein their properties and functionalities are significantly influenced by imperfections alongside their inherent molecular components. Nevertheless, challenges related to the accurate characterization of defects, as well as issues pertaining to reproducibility, continue to pose substantial barriers in this field. These obstacles, coupled with the ambiguous role of various synthetic parameters in the defect formation process, impede chemists from fully realizing and leveraging the extensive potential that reticular synthesis presents.[26]

In this study, we report the synthesis and structural characterization of a novel series of Al-MOFs, designated as AlDMDA-68, using a high-yield imine-based dicarboxylic ligand, H_2DMDA. Employing a conventional heating method, a scalable and efficient approach was developed to produce AlDMDA-68 with a **rad** net analogous to that of MIL-68. The synthesis was optimized by varying M/L ratios, temperature, and reaction time, resulting in multiple Al-MOF variants. Powder X-ray diffraction (PXRD) confirmed the formation of the frameworks, while scanning electron microscopy (SEM) revealed a rod-like morphology and size variations influenced by M/L ratios. Solid-state ^{27}Al MAS NMR identified diverse aluminum coordination environments, indicating the presence of framework defects. BET analysis revealed a high surface area of 1866 $m^2\ g^{-1}$ and significant nitrogen uptake (~777 $cm^3\ g^{-1}$), with pore sizes of 15.5 Å, 18.4 Å, and 31.6 Å, indicating a hierarchical microporous–mesoporous architecture. Thermogravimetric analysis (TGA) and variable-temperature PXRD confirmed thermal stability up to ~350 °C. Furthermore, a five-fold scale-up of compound AlDMDA-68 confirmed the reproducibility and potential for large-scale synthesis. These findings establish AlDMDA-68 as a promising candidate for various potential applications due to its large porosity and defect-engineered functionality.

Experimental

Chemical reagents

4,4′-(Hydrazine-1,2-iylidenebis(methanylylidene))dibenzoic acid (H_2DMDA) was prepared by reported procedure.[24] Anhydrous aluminum chloride ($AlCl_3$) (≥98.0%, Merck), dimethylformamide (DMF) (≥99.0%, Merck),

diethylformamide (DEF) (≥99.0%, Merck), ethanol (EtOH) (≥99.0%, ECHO), acetone (≥99.0%, Merck), hydrazine (35 wt% in H_2O) (≥99.0%, Aldrich), and terephthalaldehydic acid (≥98.0%, TCI) were all used as received.

Synthesis of H_2DMDA

In a round-bottom flask, terephthalaldehydic acid (6.305 g, 42 mmol) was dissolved in 300 mL of ethanol. The solution was heated and stirred in an oil bath at 60 °C under atmospheric conditions for a duration of 10 min until it attained a clear appearance. Hydrazine (35 wt% in H_2O) (1.83 mL, 20 mmol) was added to the solution slowly; during this process, the solution transitioned from clear to yellow. The mixture was then refluxed at 70 °C for 2 h, after which it was allowed to cool. The product, H_2DMDA, is collected through vacuum filtration and rinsed with ethanol. The final pale-yellow colored product (yield: 86%) was dried at 55 °C for 24 h and stored for further experiments. ^{1}HNMR (400 MHz, DMSO-d^6); δ ppm: 8.7 (s, 2H), 8.0 (d, 4H), 7.9 (d, 4H).

Synthesis of AlDMDA

Anhydrous $AlCl_3$ (0.030 g, 0.225 mmol) and H_2DMDA (0.053 g, 0.18 mmol) were combined in 10 mL of DEF in a round-bottom flask, which was subsequently equipped with a condenser. The mixture was subjected to heating and stirring under atmospheric pressure at 120 °C for 24 h at 400 rpm to yield the as-synthesized product. The as-synthesized product was washed with DMF, changed three times to remove unreacted ligands, followed by centrifugation with acetone three times, and dried in a vacuum at 90 °C for 12 h.

Results and discussion

Our research aimed at developing highly porous aluminum-based MOF, specifically AlDMDA-68, commenced with the synthesis of dicarboxylic ligands: 4,4′-(hydrazine-1,2-iylidenebis(methanylylidene))dibenzoic acid (H_2DMDA) by the reported procedure.[24] The target ligands were successfully synthesized with a high yield. Characterizations were achieved through ^{1}H NMR and IR spectroscopy, all of which confirmed the formation of the imine-based ligands (Fig. S2 and S3). The formation of AlDMDA was achieved through the application of conventional heating, specifically reflux. Conventional heating methods represent an effective approach for the large-scale synthesis of MOFs, particularly when compared to traditional techniques such as solvothermal synthesis.[27] However, these methods often require elevated temperatures, which can pose challenges for degradable ligands. Specifically, imine-based ligands are susceptible to dissociation under such extreme conditions, with the potential for hydrolysis to lead to the regeneration of the starting materials.[28] We meticulously optimized our synthesis process to address these issues by varying the metal-to-ligand ratios, temperature profiles, and reaction times to achieve the desired product. Using a conventional heating method, a novel aluminum Al-MOF was prepared when initiating a synthesis involving a combination of Al(III) salts with corresponding imine ligands. Following the completion of the reaction process, MOFs with porous structures typically retain guest molecules, including unreacted linkers, uncoordinated metal precursors, or organic solvents, within their pores. These guest molecules often contribute to the stability of the pore structure. Therefore, an appropriate activation method is crucial for removing these guest molecules, thereby ensuring the stability of the pore structure. In this regard, we first subjected the as-synthesized materials to a washing procedure using DMF, followed by treatment with acetone. Subsequently, the samples were dried at 90 °C under vacuum for 12 h. This treatment resulted in the formation of hierarchically porous isomers, designated as AlDMDA-68, characterized by powder X-ray diffraction (PXRD) and BET.

Previous investigations have suggested that Al-Tz-68 may exhibit structural configurations akin to those of the well-established MIL-68 (1,4-BDC) MOF.[22] Leveraging our extensive knowledge of the properties and behaviors of AlTz-68, we decided to explore anhydrous aluminum chloride as a precursor from the variations indicated by experimental studies. This strategic decision prompted the synthesis of AlDMDA-68, which was subsequently characterized using PXRD. The crystalline material AlDMDA-68 exhibited notable diffraction signals at angles of 2.7°, 5.4°, 8.1°, and 10.8° (Fig. 3a). These signals align closely with the theoretical diffraction pattern for the Al-Tz-68 structure, indicating that AlDMDA-68 possesses a framework akin to the AlTz-68 and AlPDA-68-like **rad** net structure.[23,29]

In AlDMDA-68, each aluminum ion (Al(III)) demonstrates hexa-coordination, engaging with four oxygen atoms that originate from the carboxylate groups of the imine ligands, in addition to two oxygen atoms derived from the bridged-hydroxide group. The coordination environment of the carboxylate ligand is characterized as μ_4-bridging, as each carboxylate group coordinates to bridge two aluminum cations (Fig. 1a). This arrangement yields an octahedral configuration [AlO_6] (Fig. 1b), resulting in the formation of a one-dimensional inorganic chain propagating along the *c* direction (Fig. 1c). This one-dimensional inorganic chain is recognized as a significant metal cluster within porous Al-MOFs, establishing connections with the organic coordinating ligand to create a three-dimensional network structure (refer to Fig. 1d). This network contains two distinct types of one-dimensional channels: a triangular channel featuring micropores (as depicted in Fig. 1e) and a hexagonal channel exhibiting mesopores (illustrated in Fig. 1f).[3,22,23]

Following the activation process, AlDMDA-68 manifests a lamellar-shaped aggregated morphology (Fig. 2b), closely resembling that of CYCU-3. The particle size of AlDMDA-68 is approximately 550 ± 50 nm. The activated AlDMDA-68 was heated to 200 °C under a vacuum of 10^{-5} Torr at the degas port of the Surface Area Analyzer. This meticulous procedure aimed to effectively eliminate any solvent guest molecules

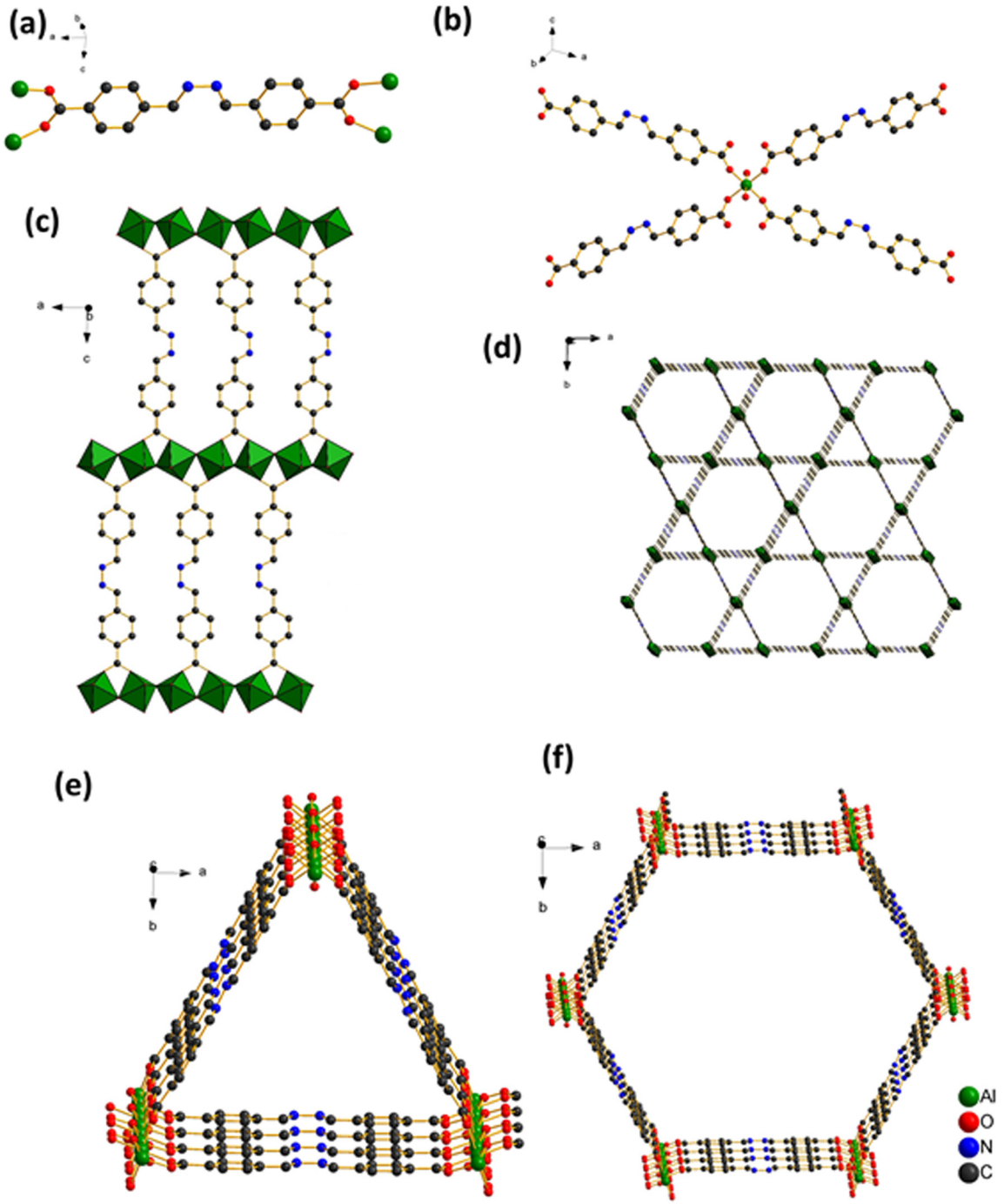

Fig. 1 (a) The coordination environment of the H_2DMDA ligand in the AlDMDA-68. (b) The aluminum ion in AlDMDA-68 is coordinated in an octahedral arrangement. (c) Coordination modes of one-dimensional inorganic chains and their ligands. (d) A 3D structure of AlDMDA-68. (e) Microporous triangular window channels of AlDMDA-68. (f) Mesoporous hexagonal window channels of AlDMDA-68.

that may have been entrapped within the intricate pores of the material. Upon completion of the solvent removal, ~65 mg of the sample was transferred to the analysis port, where nitrogen adsorption was subsequently measured at 77 K. The analysis indicated that the adsorption volume for AlDMDA-68 was approximately 777 cm^3 g^{-1}, signifying a considerable capacity for nitrogen uptake (Fig. 2c). The Brunauer–Emmett–Teller (BET) surface area was determined to be 1866 m^2 g^{-1}. Furthermore, by applying density functional theory (DFT), the pore size distributions of AlDMDA-68 were elucidated, revealing various pore sizes of 15.5 Å, 18.4 Å, and 31.6 Å (Fig. 2c (see inset)). The findings underscore the compound's dual-pore architecture, characterized by a complex arrangement of both micropores and mesopores, which aligns well with the results of the structural analysis.

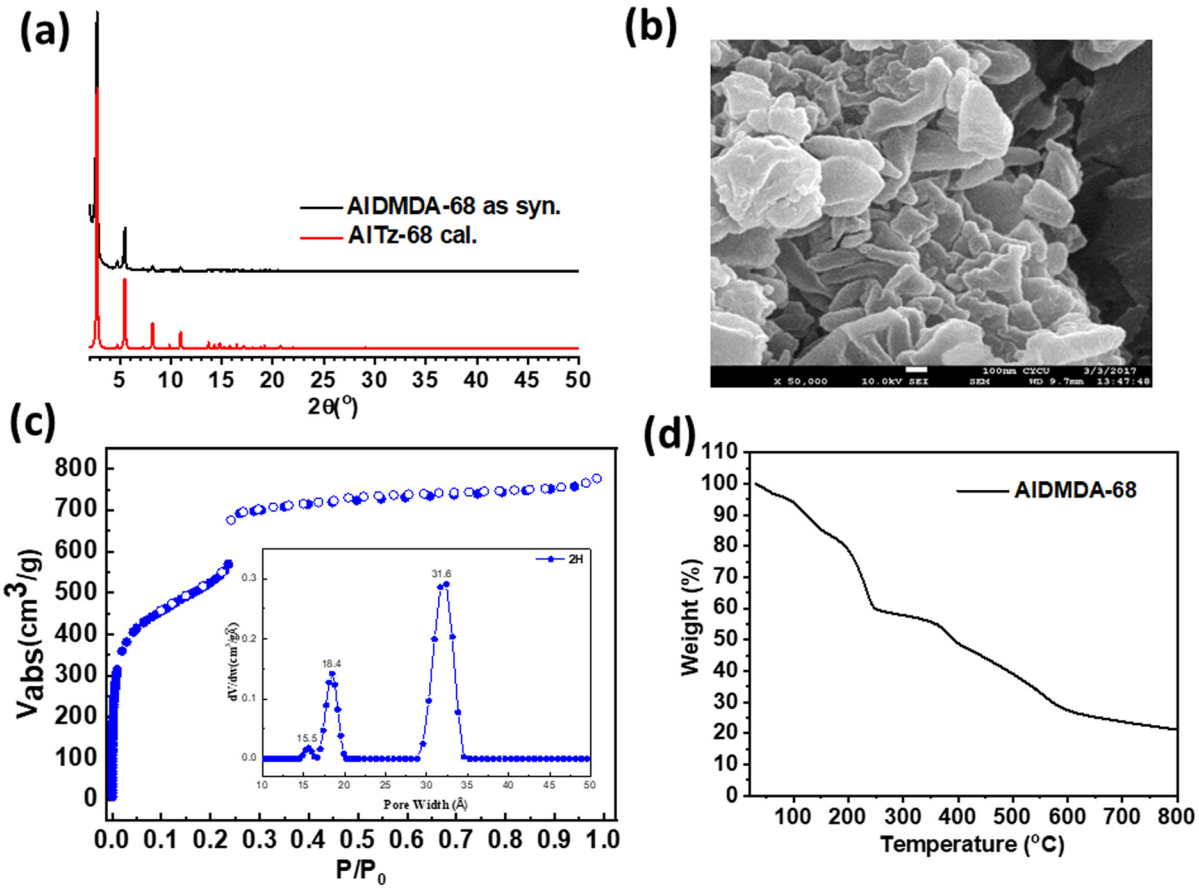

Fig. 2 (a) PXRD of AlDMDA-68. (b) SEM images of AlDMDA-68. (c) N_2 sorption isotherms of AlDMDA-68 (inset: pore size distribution of AlDMDA-68). (d) TGA curve of AlDMDA-68.

The crystal structure refinement of the sample was carried out using the Rietveld method implemented in GSAS-II, based on least-squares fitting of the full powder diffraction pattern. The structural model employed corresponds to an orthorhombic system with space group *Cmcm*. The refined lattice parameters are: a = 37.48(8) Å, b = 64.93(7) Å, and c = 6.474(9) Å (Fig. S6). The calculated diffraction pattern shows good agreement with the experimental data, particularly in the positions and intensities of the major diffraction peaks, indicating that the chosen structural model is suitable for describing the observed experimental results.

Furthermore, the crystal structure analysis of AIDMDA-68 was performed using the EXPO2 software (version 2.3.8, built on April 14, 2025),[30] employing the Le Bail method for full-pattern fitting to determine the space group and refine the unit cell parameters (Fig. S7). The best match was found to be an orthorhombic structure with the space group *Cmcm*. Within the diffraction angle range of 1.5° to 50°, no diffraction peaks were observed that could not be indexed by the *Cmcm* structure, and no impurity phases were detected.

The fitting inset presents a magnified view of the diffraction pattern in the 1.5° to 25° 2θ range, with the *Y*-axis plotted on a logarithmic scale to highlight low-intensity features. As shown, the calculated peak positions agree well with the experimental data, and no extraneous signals were observed, confirming the reliability of the structural fitting.

The thermal stability of the imine-based MOF, specifically AlDMDA-68, was evaluated using thermogravimetric analysis (TGA). The TGA results, illustrated in Fig. 2d, reveal significant mass loss for AlDMDA-68 at 350 °C due to guest solvent molecules. Beyond this temperature, it experiences a complete structural decomposition at 400 °C. These temperature thresholds indicate that the framework begins to decompose under elevated temperatures, leading to a reduction in its structural integrity. In general, the thermal stability of various Al-MOFs, which can endure temperatures nearing 450 °C, can be primarily attributed to the strong coordination interactions between metal centers and the ligand frameworks. These robust metal-to-ligand interactions contribute significantly to their overall structural stability.[28]

We have conducted an in-depth investigation into the synthesis of Al-MOF with varying M/L ratios, employing general heating methods. The literature suggests that modifying the coordinating ligands and synthesis parameters can significantly enhance the defect properties of these MOFs, thereby improving their performance across a range of applications, including gas storage, catalysis, and separation processes. In our study, we systematically adjusted the M/L

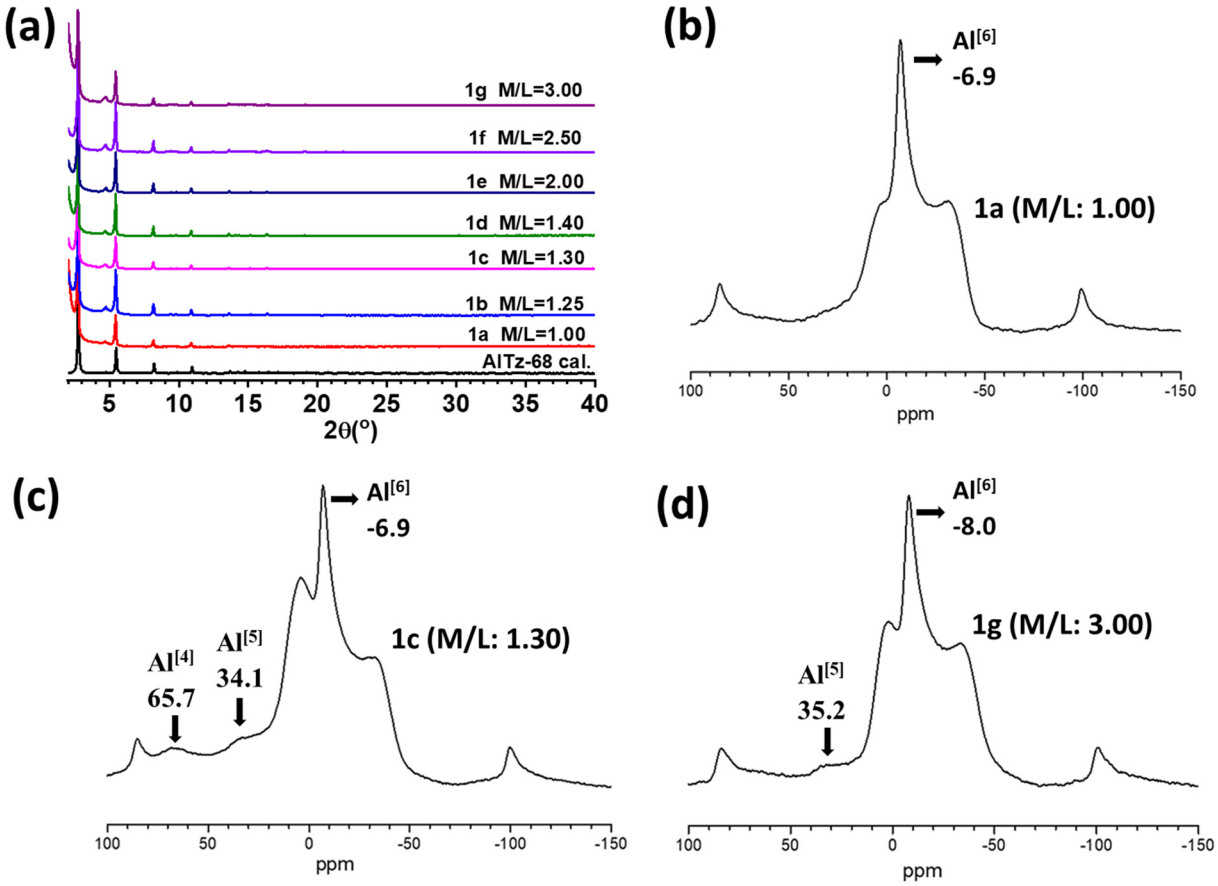

Fig. 3 (a) PXRD analysis of AlDMDA-68 at various metal-to-ligand (M/L) ratios. ^{27}Al NMR spectra of AlDMDA-68 (different M/L ratio) of (b) **1a**; (c) **1c**; (d) **1g**.

ratios, while maintaining a constant ligand concentration of 0.18 mmol and a solvent volume of 10.0 ml of diethylformamide (DEF). Various amounts of aluminum chloride ($AlCl_3$) were utilized as the metal precursor, leading to the synthesis of compounds designated as **1a** through **1g** (Table S1). The synthesis was carried out under atmospheric pressure at a consistent temperature of 120 °C for 24 hours, during which the reaction mixture was stirred continuously to ensure homogeneity. We employed a method to activate the synthesized products that involved washing them in DMF for three times to ensure the thorough removal of any unreacted ligand. Subsequently, we performed centrifugal washing with acetone three times to further purify the products, followed by drying at 90 °C for an additional day to attain the final activated compounds. Post-activation, we performed X-ray diffraction analysis on the synthesized compounds (**1a**, **1b**, **1c**, **1d**, **1e**, **1f**, and **1g**) over a range of diffraction angles from 2° to 40°. The resulting diffractograms were compared to the theoretical spectra for AlTz-68 (as shown in Fig. 4a). The significant peaks observed at 2.7°, 5.4°, 8.1°, and 10.8° corroborated the theoretical predictions, confirming the successful synthesis of AlDMDA with varying M/L ratios under the employed heating conditions. Scanning electron microscopy (SEM) analyses revealed that compounds exhibited a rod-like morphology (Fig. S4).

The particle sizes of the compounds were measured, with **1a**, **1b**, **1c**, **1d**, **1f**, and **1g** showing an average size of approximately 550 ± 50 nm, while compound **1e** was notably larger, at about 700 ± 100 nm. In this study, Solid-State Nuclear Magnetic Resonance (SS NMR) spectroscopy was employed to investigate the defect nature of Al-MOFs. Utilizing ^{27}Al Magic Angle Spinning (MAS) NMR experiments allowed for a detailed examination of the local coordination environments surrounding aluminum ions within various MOF structures. The analysis of the ^{27}Al-NMR spectrum revealed several distinct coordination forms of aluminum, each characterized by specific chemical shifts. For instance, six-coordinate aluminum ions exhibited chemical shifts ranging from approximately −10 ppm to +10 ppm. In contrast, five-coordinate aluminum ions were identified by their chemical shift, which was found to be around +30 ppm. Additionally, four-coordinate aluminum ions showed chemical shifts in the range of +50 ppm to +60 ppm.[31] These findings provide valuable insights into the structural characteristics and local environments of aluminum within the MOFs studied, thereby enhancing our understanding of how these defects might influence the

materials' properties and functionalities. The activated compounds presented distinct aluminum coordination environments (as depicted in Fig. 3b–d and S5). Solid-state NMR analysis indicated that all compounds (**1a–1g**) predominantly featured six-coordinate aluminum centers. In addition, a minor presence of five-coordinate aluminum species was detected in compounds **1b**, **1c**, **1e**, **1f**, and **1g**. Additionally, four-coordinate aluminum species were identified in compounds **1b** and **1c**. These findings demonstrate that Al-MOFs are likely to have defects in certain situations. Based on the ^{27}Al-NMR spectrum, it is suggested that the Al-MOFs exhibit defective characteristics under post-activation conditions. The defect may arise when one end of the coordinating group is bonded to the metal while the other end remains uncoordinated. To directly address the effect of defect concentration, we have performed additional BET surface area measurements on samples synthesized using different metal-to-ligand (M/L) ratios. Our results show a clear trend: as the M/L ratio increases, the measured surface area also increases (Fig. S8). The synthesis of MOFs can be significantly influenced by defect engineering and the suppression of interpenetration. An increased metal-to-ligand (M/L) ratio often results in an excess of metal, leading to the creation of missing linker defects where certain organic linkers are absent, yet the framework remains intact due to the presence of other linkers and metal nodes. This defect creation enhances the surface area. Furthermore, a higher M/L ratio can also favor the growth of less interpenetrated or non-interpenetrated frameworks, particularly under low ligand concentrations, thereby increasing the accessibility of pores. Consequently, both defect formation and reduced interpenetration are critical mechanisms that contribute to increased surface area in MOFs.

The PXRD pattern of AlDMDA-68 before and after N_2 adsorption shows no noticeable changes when compared to the as-synthesized material, indicating that the framework remains structurally intact throughout the activation and gas sorption processes (Fig. S9). Furthermore, the conventional heating method is characterized by its simplicity, efficiency, low energy consumption, and cost-effectiveness. It also possesses the capability for large-scale synthesis. This study undertakes a large-scale synthesis experiment utilizing an M/L ratio of 1.30 in AlDMDA-68. In this study, we successfully scaled up the synthesis of AlDMDA-68 to a fivefold increase while preserving its crystallinity (Fig. 4).

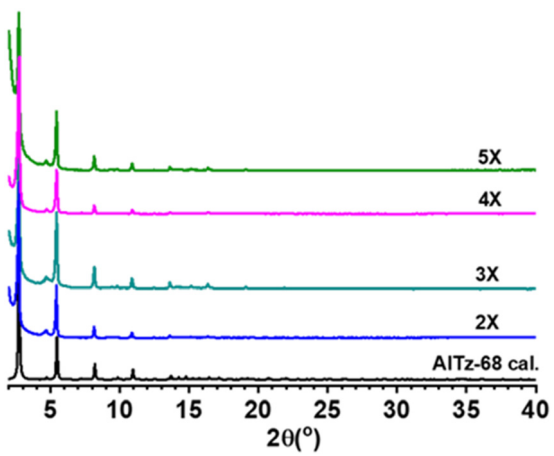

Fig. 4 PXRD patterns of AlDMDA-68 (from 1 to 5 times scale-up synthesis).

Conclusions

We have successfully designed and synthesized novel Al-MOFs with tunable mesoporosity and defect characteristics. These materials exhibit a **rad** net analogous to MIL-68 and represent a new class of non-interpenetrated isoreticular Al-MOF with well-defined mesoporous structures with high surface area. Additionally, a systematic study was conducted to investigate the influence of M/L ratios on MOF formation using a straightforward, scalable conventional heating method. A series of AlDMDA-type MOFs were synthesized and characterized. PXRD confirmed structural integrity. Solid-state ^{27}Al MAS NMR spectroscopy uncovered diverse aluminum coordination environments, indicating the presence of framework defects arising from partial ligand coordination. The mesoporosity and defect chemistry achieved through linker design and M/L tuning are expected to play a pivotal role in tailoring the functional properties of these materials. Furthermore, the synthesis was successfully scaled up fivefold without compromising structural features, highlighting the practical applicability of the approach. For the upscaled reaction, we maintained the same reaction conditions as in the small-scale synthesis, including temperature, time, and reagent ratios. The reaction vessel was lowered into a preheated oil bath at 120 °C, as also used in the small-scale procedure. In the upscaled synthesis, we used appropriately larger round-bottom flasks (50 mL or 100 mL), depending on the total solvent volume, to accommodate the increased reaction mixture while maintaining efficient stirring and heat transfer. The AlDMDA-68 MOF shares structural similarities with our previously reported Al-based mesoporous MOFs, such as AlTz-68 and AlPDA-68; however, it presents both advantages and disadvantages in comparison. One notable advantage is the ease and cost-effectiveness of ligand synthesis—the H_2DMDA ligand is readily prepared from commercially available and inexpensive precursors, making the overall process more scalable. In contrast, the ligand used in AlTz-68 is more synthetically demanding. On the other hand, a key disadvantage of AlDMDA-68 is the ligand's susceptibility to hydrolysis, which can compromise the chemical stability of the framework, especially under humid or aqueous conditions. Additionally, AlDMDA-68 exhibits a lower BET surface area compared to AlTz-68 and AlPDA-68, which may limit its performance in applications requiring high porosity. Despite these limitations, AlDMDA-

68 maintains a comparable thermal stability to the previously reported Al-MOFs, confirming its structural robustness under elevated thermal conditions. Therefore, this work lays the foundation for developing advanced Al-MOFs for various potential applications.

Author contributions

Souvik Pal; Ling-I Hung; Wun-Jing Chen: investigation, formal analysis, data curation, writing – original draft. Chun-Chuen Yang: Rietveld refinement. Jiun-Jen Chen and Chia-Her Lin: writing – review & editing, supervision, resources, conceptualization.

Conflicts of interest

There are no conflicts to declare.

Data availability

Supplementary information is available: The data supporting the findings of this study are available within the manuscript and its SI. Additional datasets, including raw PXRD patterns, NMR spectra, sorption isotherms, and TGA curves, are available from the corresponding author upon reasonable request. See DOI: **https://doi.org/10.1039/D5CE00532A**.

Acknowledgements

This research was supported by the National Science and Technology Council with grant numbers: NSTC 113-2113-M-003-015-MY2.

Notes and references

1 S. Pal, S. Kulandaivel, Y.-C. Yeh and C.-H. Lin, *Coord. Chem. Rev.*, 2024, **518**, 216108.
2 K. Wang, Y. Li, L.-H. Xie, X. Li and J.-R. Li, *Chem. Soc. Rev.*, 2022, **51**, 6417–6441.
3 S.-H. Lo, C.-H. Chien, Y.-L. Lai, C.-C. Yang, J. J. Lee, D. S. Raja and C.-H. Lin, *J. Mater. Chem. A*, 2013, **1**, 324–329.
4 S. Pal, L.-I. Hung, W.-J. Chen, J.-J. Chen, C.-C. Yang and C.-H. Lin, *J. Am. Chem. Soc.*, 2016, **138**, 15507–15509.
5 Z. Chen, S. L. Hanna, L. R. Redfern, D. Alezi, T. Islamoglu and O. K. Farha, *Coord. Chem. Rev.*, 2019, **386**, 32–49.
6 O. M. Yaghi, M. O'Keeffe, N. W. Ockwig, H. K. Chae, M. Eddaoudi and J. Kim, *Nature*, 2003, **423**, 705–714.
7 H. Jiang, D. Alezi and M. Eddaoudi, *Nat. Rev. Mater.*, 2021, **6**, 466–487.
8 Z. Chen, K. O. Kirlikovali, P. Li and O. K. Farha, *Acc. Chem. Res.*, 2022, **55**, 579–591.
9 M. Eddaoudi, J. Kim, N. Rosi, D. Vodak, J. Wachter, M. O'Keeffe and O. M. Yaghi, *Science*, 2002, **295**, 469–472.
10 D. Yuan, D. Zhao, D. Sun and H.-C. Zhou, *Angew. Chem., Int. Ed.*, 2010, **49**, 5357–5361.
11 S. Surblé, C. Serre, C. Mellot-Draznieks, F. Millange and G. Férey, *Chem. Commun.*, 2006, 284–286, DOI: **10.1039/B512169H**.
12 J. H. Cavka, S. Jakobsen, U. Olsbye, N. Guillou, C. Lamberti, S. Bordiga and K. P. Lillerud, *J. Am. Chem. Soc.*, 2008, **130**, 13850–13851.
13 A. Schaate, P. Roy, A. Godt, J. Lippke, F. Waltz, M. Wiebcke and P. Behrens, *Chem. – Eur. J.*, 2011, **17**, 6643–6651.
14 G. Férey, M. Latroche, C. Serre, F. Millange, T. Loiseau and A. Percheron-Guégan, *Chem. Commun.*, 2003, 2976–2977, DOI: **10.1039/B308903G**.
15 W. Fan, K.-Y. Wang, C. Welton, L. Feng, X. Wang, X. Liu, Y. Li, Z. Kang, H.-C. Zhou, R. Wang and D. Sun, *Coord. Chem. Rev.*, 2023, **489**, 215175.
16 B. Seoane, V. Sebastián, C. Téllez and J. Coronas, *CrystEngComm*, 2013, **15**, 9483–9490.
17 K. Barthelet, J. Marrot, G. Férey and D. Riou, *Chem. Commun.*, 2004, 520–521, DOI: **10.1039/B312589K**.
18 C. Volkringer, M. Meddouri, T. Loiseau, N. Guillou, J. Marrot, G. Férey, M. Haouas, F. Taulelle, N. Audebrand and M. Latroche, *Inorg. Chem.*, 2008, **47**, 11892–11901.
19 A. Fateeva, P. Horcajada, T. Devic, C. Serre, J. Marrot, J.-M. Grenèche, M. Morcrette, J.-M. Tarascon, G. Maurin and G. Férey, *Eur. J. Inorg. Chem.*, 2010, **2010**, 3789–3794.
20 Q. Yang, S. Vaesen, M. Vishnuvarthan, F. Ragon, C. Serre, A. Vimont, M. Daturi, G. De Weireld and G. Maurin, *J. Mater. Chem.*, 2012, **22**, 10210–10220.
21 L. Mitchell, B. Gonzalez-Santiago, J. P. S. Mowat, M. E. Gunn, P. Williamson, N. Acerbi, M. L. Clarke and P. A. Wright, *Catal. Sci. Technol.*, 2013, **3**, 606–617.
22 S.-H. Lo, L. Feng, K. Tan, Z. Huang, S. Yuan, K.-Y. Wang, B.-H. Li, W.-L. Liu, G. S. Day, S. Tao, C.-C. Yang, T.-T. Luo, C.-H. Lin, S.-L. Wang, S. J. L. Billinge, K.-L. Lu, Y. J. Chabal, X. Zou and H.-C. Zhou, *Nat. Chem.*, 2020, **12**, 90–97.
23 S. Kulandaivel, C.-C. Yang, Y.-C. Yeh and C.-H. Lin, *Chem. – Eur. J.*, 2024, **30**, e202400603.
24 L. Feng, S. Yuan, J.-S. Qin, Y. Wang, A. Kirchon, D. Qiu, L. Cheng, S. T. Madrahimov and H.-C. Zhou, *Matter*, 2019, **1**, 156–167.
25 W. Xiang, Y. Zhang, Y. Chen, C.-j. Liu and X. Tu, *J. Mater. Chem. A*, 2020, **8**, 21526–21546.
26 N. S. Portillo-Vélez, J. L. Obeso, J. A. de los Reyes, R. A. Peralta, I. A. Ibarra and M. T. Huxley, *Commun. Mater.*, 2024, **5**, 247.
27 L.-I. Hung, S. Pal, T.-T. Hsu, S.-T. Tseng, T.-L. Wu, P. Berilyn So, Y.-T. Chang, S.-L. Wang, Y.-T. Wang, T.-H. Chen, C.-W. Chan, H.-T. Chen, D.-Y. Kang and C.-H. Lin, *Chem. – Eur. J.*, 2025, **31**, e202500136.
28 U. S. F. Arrozi, V. Bon, S. Krause, T. Lübken, M. S. Weiss, I. Senkovska and S. Kaskel, *Inorg. Chem.*, 2020, **59**, 350–359.
29 S. Pal, P.-Y. Lu, L.-I. Hung, C.-H. Lin and C.-F. Wang, *J. Taiwan Inst. Chem. Eng.*, 2025, **172**, 106114.
30 A. Altomare, C. Cuocci, C. Giacovazzo, A. Moliterni, R. Rizzi, N. Corriero and A. Falcicchio, *J. Appl. Crystallogr.*, 2013, **46**, 1231–1235.
31 G. A. Rosales-Sosa, A. Masuno, Y. Higo, H. Inoue, Y. Yanaba, T. Mizoguchi, T. Umada, K. Okamura, K. Kato and Y. Watanabe, *Sci. Rep.*, 2015, **5**, 15233.

